Research Article

For reprint orders, please contact: reprints@futuremedicine.com

Nanomedicine

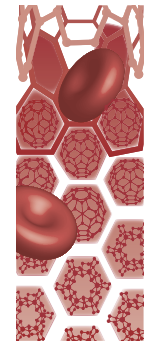

Antibody-functionalized gold nanoparticles as tumor targeting radiosensitizers for proton therapy

Sha Li[‡,1], Sandra Bouchy[‡,2], Sebastien Penninckx[‡,1], Riccardo Marega[1], Ornella Fichera[1], Bernard Gallez[3], Olivier Feron[4], Philippe Martinive[5], Anne-Catherine Heuskin[1], Carine Michiels*[,2] & Stéphane Lucas[1]

[1]Research Center for the Physics of Matter & Radiation (PMR-LARN), Namur Research Institute for Life Sciences (NARILIS), University of Namur, B-5000 Namur, Belgium

[2]Unité de Recherche en Biologie Cellulaire (URBC), Namur Research Institute for Life Sciences (NARILIS), University of Namur, B-5000 Namur, Belgium

[3]Biomedical Magnetic Resonance Group (REMA), Louvain Drug Research Institute, Université Catholique de Louvain, B-1200 Woluwé, Saint Lambert, Belgium

[4]Pole of Pharmacology & Therapeutics (FATH), Institut de Recherche Expérimentale et Clinique (IREC), UCL (Université Catholique de Louvain), B-1200 Brussels, Belgium

[5]Department of Radiotherapy & Oncology, CHU & University of Liège, B-4000 Liège, Belgium

*Author for correspondence: Tel.: +32 81 724 131; carine.michiels@unamur.be

‡Authors contributed equally

Aim: This study aimed at developing antibody-functionalized gold nanoparticles (AuNPs) to selectively target cancer cells and probing their potential radiosensitizing effects under proton irradiation. **Materials & methods:** AuNPs were conjugated with cetuximab (Ctxb–AuNPs). Ctxb–AuNP uptake was evaluated by transmission electron microscopy and atomic absorption spectroscopy. Radioenhancing effect was assessed using conventional clonogenic assay. **Results & conclusion:** Ctxb–AuNPs specifically bound to and accumulated in EGFR-overexpressing A431 cells, compared with EGFR-negative MDA-MB-453 cells. Ctxb–AuNPs enhanced the effect of proton irradiation in A431 cells but not in MDA-MB-453 cells. These data indicate, for the first time, that combining enhanced uptake by specific targeting and radioenhancing effect, using conjugated AuNPs, is a promising strategy to increase cell killing by protontherapy.

First draft submitted: 8 May 2018; Accepted for publication: 14 November 2018; Published online: 24 January 2019

Keywords: EGFR • gold nanoparticles • nanoparticle uptake • protontherapy • radiosentizing effects

Radiotherapy is mainly limited by two factors: the tolerance to the irradiation of healthy tissues surrounding tumors and tumor radioresistance. One of the main strategies proposed to improve the selectivity of radiation effects is to use targeted nanoagents able to enhance the efficacy of tumor targeting and to amplify the effects of radiations. Experimental and simulation works have demonstrated that gold nanoparticles (AuNPs) enhance the effect of radiation in combination with kilovolt (kV) photons, megavolt (MV) photons, electrons and charged particles (H^+, C^{6+}) [1–7]. AuNPs are expected to improve the effects of the radiation by their ability to increase the dose deposition in the target volume or to locally increase the temperature. Indeed, after activation by radiation, electron bursts are emitted in the close vicinity of the nanoparticles (NPs) leading to the production of water radical clusters [8,9]. These early-stage mechanisms (up to 1 s at most after interaction) are responsible for the induction of damage to biomolecules [9]. A pioneering study carried out by Hainfeld *et al.* has demonstrated the effect of AuNPs to amplify x-ray radiation effect, by using AuNP intravenous injection in mice bearing a subcutaneous mammary carcinoma: a 1-year survival of 86% with AuNPs + 250 kVp x-rays was observed compared to 20% with radiation alone [10].

Recently, great efforts have been devoted to the development of active targeting with nanoparticles, for example, through their conjugation to tumor-specific ligands [11]. The EGF receptor (EGFR) is an attractive candidate for anticancer therapy [12]. Indeed, overexpression of EGFR has been reported in many types of human carcinoma [13]

Future Medicine

and has led to the development of various EGFR-targeted therapies [14–16]. Cetuximab (Ctxb; Erbitux®) is a mouse–human chimeric monoclonal antibody that binds the EGFR with high affinity. It has been approved as a first line of treatment for metastatic colorectal cancer [17] but also in non-small-cell lung cancers as well as in head and neck cancers [18]. Also, strategies to conjugate Ctxb to other therapeutic compounds or nanoobjects have been developed.

Several studies have, for instance, reported that Ctxb-conjugated AuNPs are able to target EGFR *in vitro* and *in vivo*, leading to enhanced cellular internalization of the targeted nanoparticles and therapeutic outcomes [19–22].

To date, very few studies have yet reported the effect of tumor-targeting nanoparticles in combination with heavy particle therapy. The use of heavy particle therapy (protons or carbon ions) in clinical practice has become more prevalent over the past 20 years, driven by their attracting physical properties. Proton beam deposits most of the proton energy at the end of the proton range (Bragg peak) in a targeted volume. Tissues behind the tumor, in contrast to conventional radiotherapy, are nearly completely protected. One of our previous studies has shown that amine–PEG-functionalized AuNPs successfully enhanced the effect of radiation of 25 keV μm^{-1} protons [23]. Simulation studies showed dose possible enhancement effect by AuNPs for protons. However, an intracellular AuNP concentration at least two orders of magnitude higher than what was achieved in the latter study is needed to generate these effects [1,24]. To increase the amount of gold accumulation inside the cancer cells but also with the aim of increasing their specificity, the major goal of this work was to develop EGFR-targeting AuNPs and to probe their effects in combination with protons.

Here, we describe the successful conjugation of Ctxb to the surface of AuNPs. The binding affinity of Ctxb–AuNPs to A431 cells – a human epidermoid carcinoma cell line expressing high levels of EGFR ($EGFR^+$) – was much higher than the one to MDA-MB 453 cells – a human breast carcinoma cell line that does not express EGFR ($EGFR^-$). Furthermore, a clear radiosensitizing effect was evidenced in combination with protons.

Materials & methods

Chemical materials

All chemicals were purchased from commercial sources and used without further purification except if explicitly mentioned. Allylamine and COMU (1-cyano-2-ethoxy-2-oxoethylidenaminooxy-dimethylamino-morpholino-carbenium hexafluorophosphate) were obtained from Sigma-Aldrich, Overijse, Belgium. Water was purified using a Millipore Milli-Q water production system. Commercially available Ctxb formulation (Erbitux 2 or 5 mg ml^{-1}, Merck & Co., Darmstadt, Germany) was purified by discontinuous diafiltration in centrifugal concentrators with a molecular weight cutoff (MWCO) of 10,000 g mol^{-1} (Sartorius Vivaspin, Goettingen, Germany) and the purified antibody (Ab) was freeze-dried.

Synthesis of AuNPs & antibody conjugation

Synthesis of AuNPs coated with plasma-polymerized allylamine by plasma vapor deposition has already been reported [25]. The resulting polyallylamine-coated nanoparticles were then dispersed in acetate buffer (pH 5) under 10 min of sonication and then purified from the plasma-polymerized allylamine and NaCl excess by discontinuous diafiltration in centrifugal concentrators with an MWCO of 10,000 g mol^{-1}. Ctxb (17 mg) was dissolved in 17 ml of 0.1 M phosphate-buffered saline (PBS; pH 7.4), and then a solution of COMU at 30.5 mg in 20.4 ml of 0.1 M PBS was added. The resulting mixture was stirred at 25°C for 15 min, after that 12.35 mg of AuNPs (Au amount) was then added by using a water solution of AuNPs (11 ml) with an Au concentration of 1.12 mg/ml. The reaction was stirred at 25°C for 4 h, after which it was purified by discontinuous diafiltration against H_2O in centrifugal concentrators with MWCO of 300,000 g mol^{-1}. Purification was completed when the electrical conductivity of the filtrate was less than four-times the conductivity of the deionized water used during the discontinuous diafiltration (around 1 µS/cm). This decrease of about 2000-times in the electrical conductivity is related to the progressive removal of the salts and excess reagents (antibody, coupling agent) from the reaction mixture thanks to the membrane-based separation (Supplementary Figure 1 & Table 1). Ctxb–AuNPs were lyophilized through freeze-drying system (Alpha 2–4 LD Plus, Analis, Namur, Belgium), providing a pinkish red powder (9.57 mg). Ctxb–AuNPs were stored under inert atmosphere at 4°C for further utilization. Prior to being incubated with cells, the lyophilized nanoparticles were resuspended in cell culture medium and sonicated for 15 min.

Characterization

The size distribution of the nanoparticles was first determined by disc centrifuge (CPS Instruments Europe, Oosterhout, The Netherlands). This method estimates the 'hydrodynamic size', as measured by dynamic light scattering, to be 'the size of a hypothetical hard sphere that diffuses in a liquid in the same fashion as that of the particle being measured. In practice though, particles or macromolecules in solution are nonspherical, dynamic (tumbling) and solvated, hence the terminology, hydrodynamic diameter' [26].

Transmission electron microscopy (TEM) images were acquired with a Philips Tecnai 10 transmission electron microscope operating at 80 keV and in bright-field mode. Samples for TEM analysis were obtained by deposition of AuNPs and Ctxb–AuNPs solutions onto carbon-coated Cu grids. UV–vis spectra were recorded on a UV/vis spectrophotometer SPECORD® 205, using 1-cm path quartz or optical glass cuvettes. To assess the proportion of Ctxb conjugated to AuNPs, a set of thermogravimetric measurements, atomic absorption spectroscopy (AAS) and protein quantification assays (Thermo Scientific Pierce 660-nm assay) were conducted. Thermogravimetric analysis (TGA) was carried out with a TGA 4000 apparatus from Perkin Elmer, by treating the samples placed in Pt pans with the following procedure: isotherm at 100°C for 20 min (to remove residual solvent, if any), ramp from 100 to 1000°C at 10°C·min^{-1} air (flow rate on the sample of 90 ml·min^{-1}). The Ctxb content of the samples was quantified by plotting the calibration curve with known concentrations of Ctxb, desalted by discontinuous diafiltration of Erbitux 5 mg ml^{-1} solutions in centrifugal concentrators of 10,000 Da cutoff (Millipore Amicon 15, Burlington, MA, USA), used for external calibration. Absorbance at 660 nm of wells containing defined amounts of Au (7–8 µg Au/well, as determined by AAS) of both AuNPs and Ctxb–AuNP were recorded before and after addition of the colorimetric reagent using a spectrophotometer (X-Mark™ Microplate Spectrophotometer, BioRad, Hercules, CA, USA). Linear regression of the calibration curve, and absorbance subtraction between Ctxb–AuNP and AuNPs allowed to estimate the Ctxb content. The detailed explanation of this experimental part in proposed in Supplementary Information 2.

Cell culture

A431 cells and MDA-MB-453 cells were grown, respectively, in a Dulbecco's modified Eagle's complete medium (DMEM; 4.5 g l^{-1} D-glucose, Gibco® by Life Technologies, MA, USA) or Roswell Park Memorial Institute medium (RPMI 1640, Gibco by Life Technologies, MA, USA), containing 10% (v:v) fetal bovine serum (FBS, Gibco by Life Technologies) at 37°C in a humidified atmosphere incubator containing 5% CO_2. A431 cells are known to expressed very high level of EGFR compared with other cancer cell types [27]. It has been estimated that A431 cells display 1.2×10^6 molecules of EGFR per cell [28]. On the other hand, the literature reports that MDA-MB-453 cells are negative for this receptor [29]. In order to confirm these data, we assessed, by RT-qPCR, the mRNA level of the EGFR in the two cell lines cultivated in our laboratory and used for the experiments described in the manuscript. The cycle threshold was 18.5 for A431 cells and 31.5 for MDA-MB-453 cells, indicating a 8×10^6-fold difference.

Cell viability assay

MTS (3-(4,5-dimethylthiazol-2-yl)-5-(3-carboxymethoxyphenyl)-2-(4-sulfophenyl)-2H-tetrazolium) assay was used to measure the viability of cells incubated (or not) with Ctxb–AuNPs at different concentrations. In this study, 10,000 cells were seeded in 96-well plate. 24 h later, culture medium containing different concentrations of Ctxb–AuNPs was added. After 30 min of incubation, the cells were washed with PBS and 120 µl of culture medium containing MTS (Cell Titer 96® Aqueous One Solution Reagent, Promega, Madison, WI, USA) in a 5:1 ratio was added in each well. After 1 h of incubation with MTS tetrazolium compound, the optical density was determined at 490 nm using a spectrophotometer (X-Mark Microplate Spectrophotometer, BioRad, Hercules, CA, USA).

Surface ELISA

A431 cells or MDA-MB-453 cells were seeded at 10,000 cells per well, in 96-well plates (Costar, Sigma–Aldrich, Overijse, Belgium) 24 h prior to the ELISA test. Cells were rinsed once with PBS and then fixed 10 min with PBS containing 4% para-formaldehyde. After one wash with PBS, wells were blocked with 5% of nonfat dry milk in PBS for 1 h at room temperature. Cells were rinsed one time with PBS and one time with BSA 1% in PBS for 5 min. Ctxb or Ctxb–AuNPs were added to the cells at various concentrations for 1 h at room temperature. Plates were washed three-times with PBS–BSA, and a mouse monoclonal antihuman IgG–biotin antibody (Sigma) diluted in

10.2217/nnm-2018-0161

PBS–BSA at 1 mg ml^{-1} was added for 1 h at room temperature. Cells were washed three-times and incubated with streptavidin-alkaline phosphatase (Sigma) for 30 min at room temperature. After three washing steps with PBS–BSA and one with PBS, alkaline phosphatase activity was revealed with 1 mg ml^{-1} *p*-nitrophenylphosphate in 0.1 M diethanolamine pH 10.3 containing 1.5 mM levamisole hydrochloride. The reaction was stopped with NaOH 2 N and the surface expression was quantified spectrophotometrically, by reading the optical density (405 nm) 45 min after addition of the substrate. Since AuNPs do absorb at 405 nm, for each AuNP concentration interfaced with cells, corresponding wells without cells but with culture medium were also incubated in exactly the same experimental conditions. Afterwards, all the washing and incubation steps were performed exactly using the same procedure for wells containing cells and wells without cells. At the end, when the absorbance is measured, the absorbance of the wells without cells was subtracted from the one of the corresponding wells with cells [30].

Intracellular distribution of nanoparticles

TEM was performed to precisely localize the position of intracellular nanoparticles. Cells were first fixed for 2 h at 4°C with 2.5% (w/v) glutaraldehyde (Agar Scientific) in 0.1 M cacodylate buffer (pH 7.4). Cells were washed with cacodylate buffer and subsequently post-fixed in 1% (v/w) osmium tetroxide (Merck Chemicals, Darmstadt, Germany). Samples were dehydrated by successive passages in increasing concentration of ethanol (30, 50, 70, 85 and 100%). After embedding in epon resin LX 112 (Ladd Research Industries, Williston, VT, USA), ultrathin sections of cells were prepared for TEM analysis using an 8800 ultratome III (LKB, Thermo Fisher Scientific, Asse, Belgium). They were then stained with uranyl acetate and lead citrate. Observations were performed with an FEI Technai 10 TEM (Philips, FEI Inc., OR, USA) [31].

Cell uptake analysis by atomic absorption microscopy

To verify and quantify a possible time-dependent amount of Au internalization by the selected cell lines, a combination of cell incubation experiments, cell mineralization and mineralized samples analysis by AAS was carried out. To avoid possible interferences of serum components into the targeting properties of the materials, the incubations occurred under serum-free conditions.

Briefly, A431 and MDA-MB-453 cells were incubated with 5 µg Au ml^{-1} of AuNPs (Au amount) in a FBS-free medium for 30 min at 37°C under 5% CO_2. After incubation, cells were first washed with cell medium, then with PBS and finally trypsinized at 37°C. Detached cells were resuspended in complete cell medium and centrifuged. The actual number of cells in each sample was then determined using a cell counter (Countess Automated Cell Counter, Invitrogen, Carlsbad, CA, USA). After the centrifugation, the medium was discarded, and the cells were digested using 1 ml of aqua regia (37 wt% HCl, 65 wt% HNO_3; Sigma-Aldrich) overnight. The Au content of the samples was quantified using an atomic absorption spectrophotometer (AA-7000F from Shimadzu) by plotting the calibration curve with known concentrations of an Au standard solution (Merck Chemicals, Belgium) used for external calibration. Triplicate readings were analyzed for each sample. The amount of Au detected into the cells was expressed as internalized Au quantity (pg) per cell.

Proton irradiation

Detailed protocols were described in our previous report [23]. Briefly, 24 h before irradiation, the sterilized home-made irradiation chambers were pretreated 20 min with 15 µl of human fibronectin (PHE0023, Gibco by Life Technologies, MA, USA) to allow cell adhesion. Then, 40,000 of either A431 or MDA-MB-453 cells were seeded as a 32-µl drop at the center of the irradiation chambers. These irradiation chambers were then closed with a plastic cap to avoid dehydration and contamination and were placed in an incubator at 37°C with 5% CO_2. 2 h after seeding, the drop was rinsed twice with PBS to remove nonadherent cells. For both cell lines, attached cells formed monolayers. The irradiation chambers were then filled with FBS-free medium (control group) or with FBS-free medium containing 5 µg Au ml^{-1} of Ctxb–AuNPs and placed in the incubator for 30 min.

On the day of irradiation, the medium was discarded from the irradiation chamber, the plastic cap was removed and a sterile cotton swab was used to take away the cells, which may have diffused outside the irradiation field. The irradiated chamber was then closed with the plastic cap, rinsed with PBS and filled with CO_2-independent medium (Gibco by Life Technologies, MA, USA).

The cell monolayer was irradiated with a homogenous broad proton beam defocused over 1 cm^2 area, produced by a 2 MV Tandem accelerator (High Voltage Engineering Europa). The reader is referred to [32] for a thorough description of the experimental setup and the irradiation procedure. Briefly, 1.3 MeV pristine proton beam was

extracted in air through a 1-μm silicon nitride window. The linear energy transfer (LET) at the cell sample location was computed using SRIM software [33], using three stacked layers representing the setup: 1 μm Si_3N_4 exit window, a small 3 mm air gap between the exit window and the cell dish, and the 3 μm mylar foil constituting the bottom of the irradiation dish. The energy of transmitted particles was averaged and the LET was obtained for this average proton energy. In this study, a 25 keV μm^{-1} LET value, corresponding to an energy of 1.3 MeV in vacuum, was chosen to obtain the maximum relative biological effectiveness for a proton beam for A431 cells as determined in Li *et al.* [23]. The irradiation chambers were placed vertically on a sample holder fixed at the end of the beamline. Cell samples were thus positioned perpendicularly to the incoming beam. Homogeneity was achieved by defocusing the beam and checked using a passivated implanted planar silicon detector moved along x and y directions. Dose rate was assessed every millimeter in a 1 cm^2 surface with errors less than 5% in the cell sample region. The dose rate was fixed to 2 Gy min^{-1} and the particle flux was accordingly adjusted using the classic broad beam formula [34] as shown below (Equation 1):

$$D = \frac{1.610^{-9}\ LET \varnothing}{\rho} \qquad \text{(Equation 1)}$$

Here, the density ρ is taken as 1 g cm^{-3} and Φ is the proton beam flux in part cm^{-2} s^{-1}. The dose range was chosen to cover survival fraction down to 1%.

Clonogenic assay

Immediately after irradiation, cells were detached using trypsin and the cell numbers were counted. The cell numbers were counted by Moxi™ Z-automated cell counter (Orflow). It provides an assessment of cell culture viability to report the standardized Moxi Viability Index (MVI). MVI is a ratio of the cell population of interest relative to the entire particle distribution in that sample, factoring in dead cells that have shrunken or broken apart as well as other debris and contaminants in the sample. In this work, all the cell samples had a MVI ≥ 0.90.

In order to obtain countable colony numbers for different doses of irradiation, different numbers of cells were seeded in six-well plates containing DMEM medium (A431) and RPMI (MDA-MB-453) supplemented with serum and penicillin/streptomycin and incubated at 37°C with 5% CO_2. 8 (A431) and 11 (MDA-MB-453) days postirradiation, respectively, colonies were stained with violet crystal in 2% ethanol. The numbers of visible colonies (containing 50 or more cells) were considered to represent surviving cells and were manually counted. The plating efficiency (PE) was determined for each dose of irradiation and calculated by dividing the number of colonies by the initial number of seeded cells. The surviving fraction was obtained as the ratio of the PE for the irradiated cells to the PE for control cells. The control cells underwent the exact same procedure, including the trypsinization step, except the irradiation step. At least three independent experiments were performed for each condition and the errors were evaluated as standard deviation (S.D.).

The efficiency of Ctxb–AuNPs to amplify radiation-induced A431 cell death was evaluated by calculating the sensitization enhancement ratio (SER):

$$SER(NPS) = \frac{D_{10\%}^{control}}{D_{10\%}^{NPs}}$$

Here, the $D_{10\%}^{NPS}$ and $D_{10\%}^{control}$ represent the dose required to achieve 10% surviving fraction for cells preincubated with nanoparticles and without nanoparticles, respectively.

DMSO treatment

Immediately prior to irradiation, the irradiation chambers were filled with CO_2-independent medium containing 1 M DMSO or just the medium for control samples. Studies have shown that this concentration is nontoxic for a short duration [4]. Cells were irradiated with a proton beam of 25 keV μm^{-1}, at a dose rate of 2 Gy min^{-1}. Directly after the irradiation, cells were trypsinized for clonogenic assays.

10.2217/nnm-2018-0161

Statistical analysis

All of the experiments were repeated in triplicate on separate days. All curve fittings were performed with OriginLab® software (Northampton, USA). A linear-quadratic equation was used to fit clonogenic assay data:

$$SF = e^{-(\alpha D+\beta D^2)}$$

Where SF is the surviving fraction of the cells; α and β define the linear and the quadratic components, respectively, and D is the deposited dose.

To evaluate the differences between the experimental and corresponding control samples, the data were analyzed using analysis of variance (ANOVA) for repeated measures.

Results

AuNP synthesis & characterization

To determine both the morphology and the size distribution of the synthesized nanoparticles, AuNPs and Ctxb–AuNPs were directly deposited onto a TEM grid. The observations revealed the presence of spherical objects (the Au cores) with an average size between 3 and 5 nm and a maximum at 4 nm (Figure 1A & B, Supplementary Information 3).

Disc-centrifuge analysis showed that AuNPs display a peak centered at 4–5 nm (Figure 1C). This result is in complete agreement with the one obtained by TEM. After bioconjugation of Ctxb–AuNPs, the size distribution shows a peak at around 40 nm (Figure 1C). For the observation in TEM, the hydration layer is not present due to the sample preparation procedures involved that includes dehydratation. Furthermore, the organic part can shrink during this preparation procedure. Finally, due to the low contrast of the organic moieties (essentially composed by low atomic numbers atoms: H, C, N, O, and S compared with Au) in TEM, this part could be underestimated. Hence, the hydrodynamic diameter estimated by disc centrifuge (Figure 1C) is greater than the size estimated by TEM (Figure 1B).

Zeta potential measurement of the colloidal solutions of AuNPs showed a decrease of around 9 mV after the bioconjugation step, and that the incubation of these colloids in serum-supplemented cell culture medium determines a 'neutralization' of the zeta potential value that shifts toward 0 mV (Supplementary Information 4). The absorption spectrum of Ctxb (Figure 2A) displayed the typical proteinic signature at 280 nm (aromatic amino acids), and the characteristic absorption peak of peptide at 220 nm. Such absorption features are further highlighted in the first derivative plot (dAbs/dλ). As expected, the AuNP absorption spectrum shows the surface plasmon feature at 525 nm, characteristic of small-sized AuNPs (Figure 2B) and obviously none of the 'protein signatures' found in the derivative plot of Ctxb. In the UV–vis traces of Ctxb–AuNP, one can notice the contemporaneous presence of the surface plasmon absorbance (at 535 nm) and the protein signatures of Ctxb, as previously described for similar Ctxb–AuNP bioconjugates [30]. The approximate 10-nm redshift in the SPR peak of Ctxb–AuNP can be due to a combination of the alterations in the local refractive index owing to the presence of a layer of antibody molecules on the surface of AuNPs, and the presence of some agglomerated AuNPs, as seen in the TEM images in Figure 1B.

To assess the proportion of Ctxb conjugated to AuNPs, a set of TGA, AAS and protein quantification assays were conducted (see the detailed procedure in Supplementary Information 2). As already shown for different Ctxb-nanomaterial bioconjugates [30,35,36], TGA is a useful tool to discriminate between the organic and inorganic moieties of nanomaterials. TGA of Ctxb shows a decomposition occurring in the range between 100 and 800°C, with a residual weight at 950°C close to 0%, while AuNPs typically show decomposition between 100 and 500°C, due to the polyallylamine moiety (around 30 wt%, thus ~5.0 μmol allylamine mg^{-1} of AuNPs). Ctxb–AuNPs TGA plots clearly indicate an augmented weight loss (around 60%), which is thus also due to the Ctxb loading. Most importantly, the TGA provides direct estimation of the Au amount in each sample, which is related to the residual weight found in both AuNPs (around 70%) and Ctxb–AuNP (40–45 wt%, depending on the batches). Next, a colorimetric assay based on external calibration curve with Ctxb, and wells incubated with the same Au amounts for both AuNPs and Ctxb–AuNP, revealed very similar composition findings (Supplementary Information 2 & 5). By these assays, it was possible to estimate the average product composition of Ctxb–AuNPs as 32 wt% (± 9 wt%) Ctxb, 47 wt% (± 6 wt%) for gold and 21 wt% (± 3%) for polyallylamine (n = 6). It should be pointed out that all of the following biological studies rely on the use of aliquots originating from stock solutions where the exact Au amount was determined by AAS, for both AuNPs and Ctxb–AuNP. Nonetheless, these composition values can

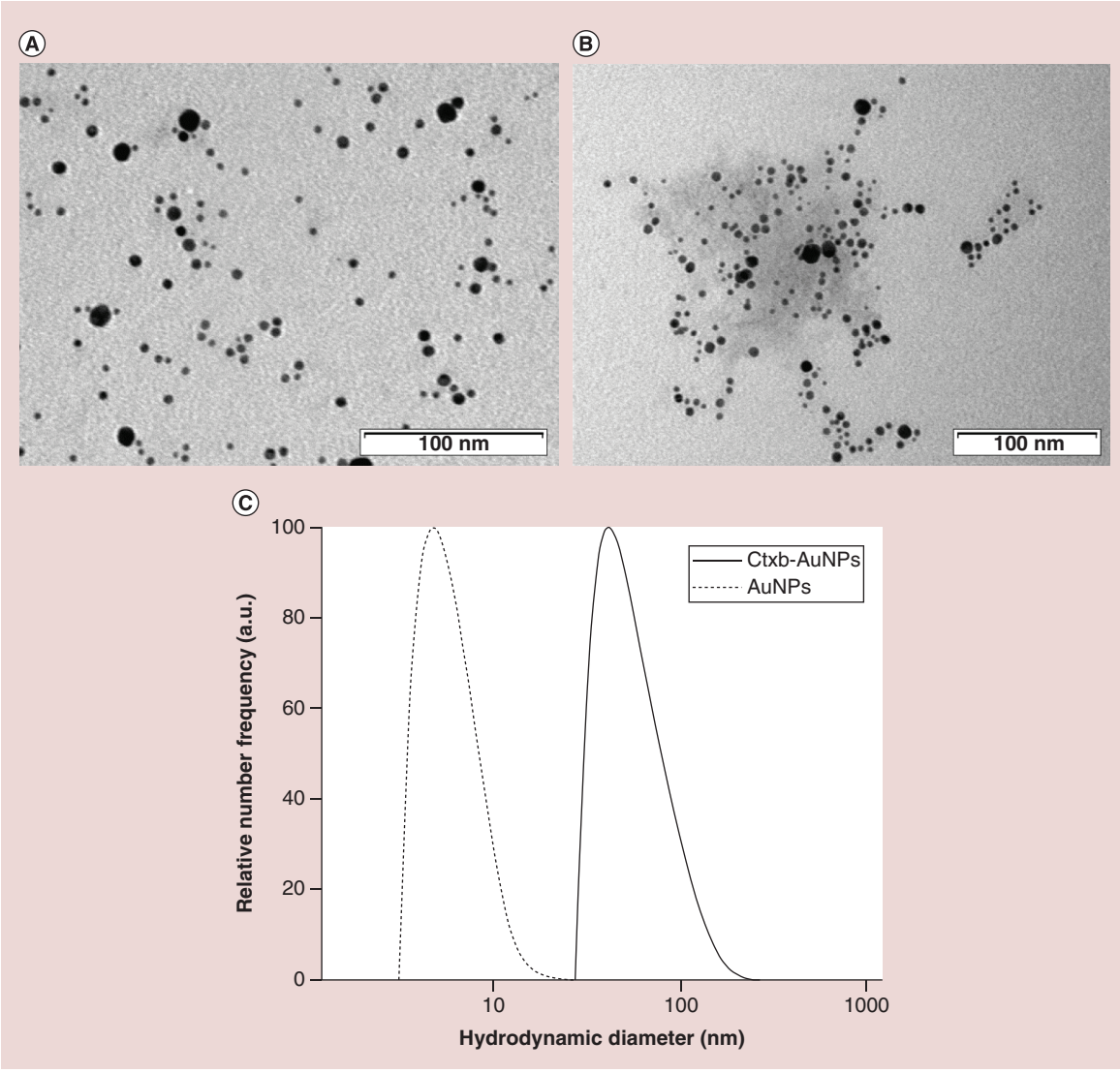

Figure 1. Characterization of gold nanoparticles and gold nanoparticles conjugated with cetuximab. TEM images of AuNPs **(A)** and Ctxb–AuNPs **(B)**, scale bar: 100 nm. **(C)** Size distribution of AuNPs before bioconjugation and after bioconjugation analyzed by analytical disc centrifuge (a.u. = arbitrary units).
AuNP: Gold nanoparticle; Ctxb: Cetuximab; TEM: Transmission electron microscopy.

be used to prepare solutions with equivalent Ctxb amounts to those determined in the Ctxb–AuNP ones, useful for the biological studies (ELISA, cytotoxicity, proton irradiation), and to estimate the number of Ctxb molecules per AuNPs. In this latter case, recent literature shows how, after performing site-oriented coupling procedures, it is possible to investigate at the microscopic scale (TEM imaging) the precise antibody loading and orientation [35]. In our case, we used the bulk composition values to estimate the average number of Ctxb molecules per particle (for a given AuNPs diameter), in line with the report by Kao *et al.* [22], who performed a similar quantification study.

It should be pointed out that this is an averaged (and thus only indicative) assessment, due to the nonoriented coupling procedure, the polydispersity of AuNPs and the probability of having a distribution also in terms of the actual number of Ctxb molecules coupled to AuNPs having the same size. By a series of assumptions and cross comparison between the compositional data, calculations, size distribution values and by comparison with literature findings, we estimate to have diameter-dependent loading of Ctxb/AuNPs that, for the most frequent sizes of 5 and 6 nm falls in the range of a theoretical ratio of 2–3 antibody molecules/nanoparticle (Supplementary Information 5).

10.2217/nnm-2018-0161

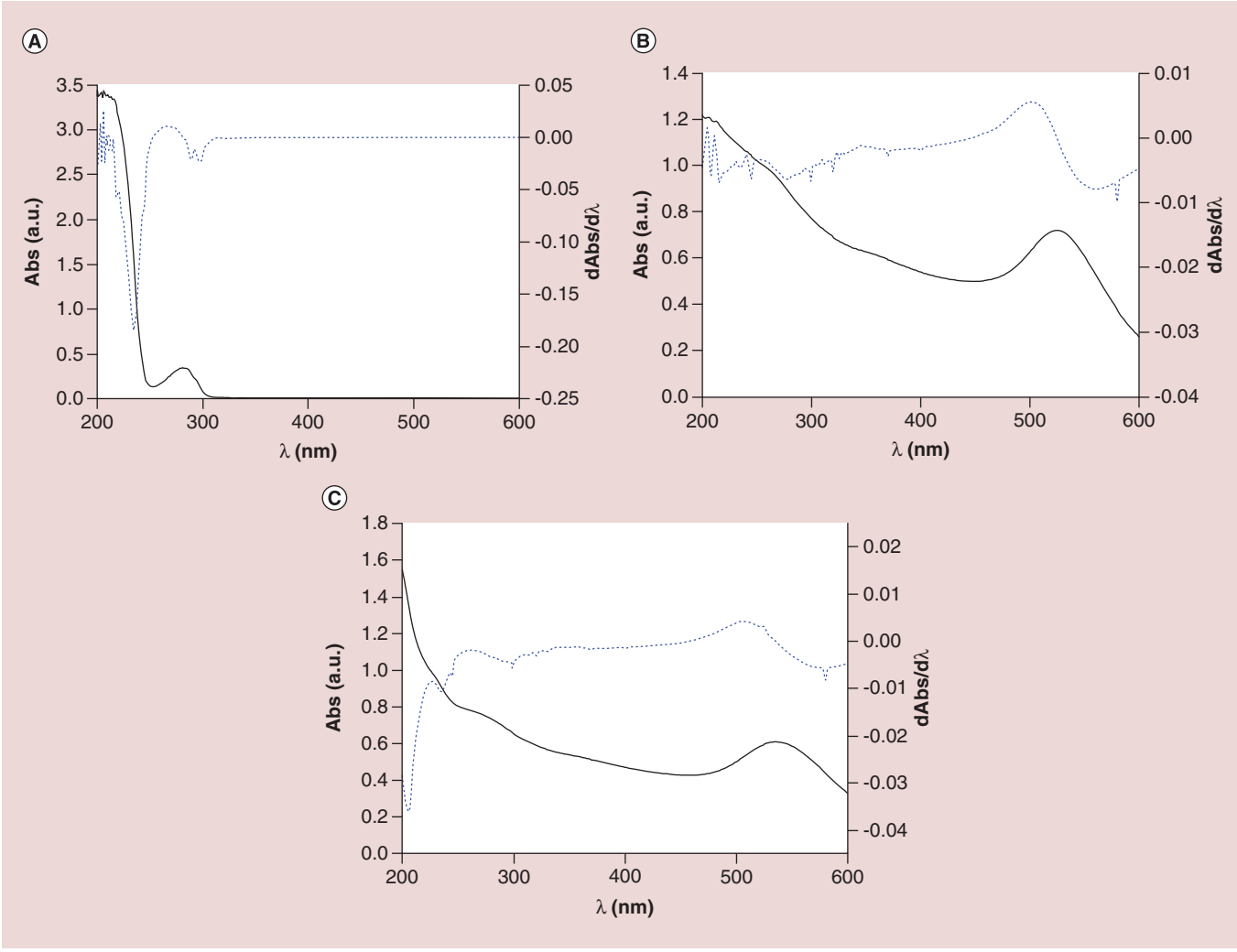

Figure 2. Characterization of AuNPs and Ctxb–AuNPs. Steady-state UV–vis absorption spectra (solid line) and derivative plots dAbs/dλ (dot line) for cetuximab **(A)**, AuNPs **(B)** and Ctxb–AuNPs **(C)**.
AuNP: Gold nanoparticle; Ctxb: Cetuximab.

In vitro evaluation of EGFR targeting

An ELISA was used to examine the relative binding affinity of Ctxb–AuNPs toward EGFR-overexpressing cells. To this end, different concentrations of Ctxb and of Ctxb–AuNPs were tested both on $EGFR^+$ and $EGFR^-$ cells (Figure 3).

As expected, Ctxb bound to $EGFR^+$ cells in a concentration-dependent manner. On the other hand, there was no binding to $EGFR^-$ cells. In our experimental setup, Ctxb binding saturated at a concentration of 0.32 μg ml^{-1} that corresponds to around 7×10^{14} Ctxb molecules per ml or 5×10^6 Ctxb molecules per A431 cell. Interestingly, Ctxb–AuNPs also bound to $EGFR^+$ cells in a concentration-dependent way. Moreover, the binding increased almost linearly with the concentration of Ctxb without saturation in the studied concentration range, suggesting the retention of the correct antibody conformation for the epitope selection and interaction in Ctxb–AuNPs conjugates. A small portion of unspecific binding of Ctxb–AuNPs to $EGFR^-$ cells was also observed. The washing process for removing NPs absorbed to the cell surface involved the step of centrifugation in order to replace the cell medium containing nanoparticles by fresh cell medium. However, during this step, some nanoparticles can be centrifuged together with the cells and thus absorbed to the cell surface by unspecific binding.

However, with the same concentration of Ctxb, a more important binding toward $EGFR^+$ cells was observed with Ctxb molecules compared with Ctxb–AuNPs. Marega *et al.* hypothesized that the spatial distribution is

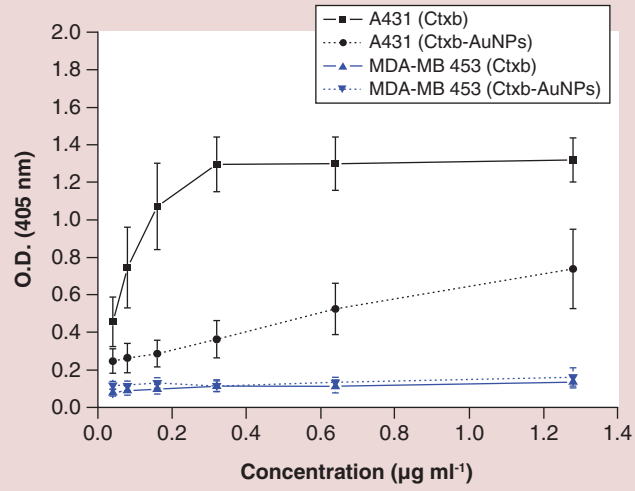

Figure 3. Surface ELISA for cetuximab and gold nanoparticles conjugated with cetuximab on EGFR$^+$ (A431) and EGFR$^-$ (MDA-MB-453) cells. The concentrations are expressed as microgram of Ctxb per milliliter. Results are presented as means ± 1 S.D. for three independent experiments.
Ctxb: Cetuximab; S.D.: Standard deviation.

constrained around nanoparticles for AuNPs conjugated with Ctxb in comparison to free Ctxb. Thus, it is possible that not all the Ctxb molecules are available to recognize the antigens that are distributed on the monolayer cell surface [30]. This could explain the apparent difference of binding affinity observed here, in other words, a lower binding of the Ctxb–AuNPs compared with free Ctxb.

Assessment of Ctxb–AuNP cytotoxicity

The cytotoxicity measurements were aimed at determining the experimental conditions to perform irradiation experiments with minimum toxicity. To investigate the toxicity of Ctxb–AuNPs, A431 cells or MDA-MB-453 cells were incubated for 30 min with Ctxb–AuNPs at different concentrations (0–100 µg Au/ml) and cell viability was assessed by a colorimetric test (MTS assay). In such an assay, viable cells produce a chromophore with absorption maxima at 490 nm, and thus absorption values are expected to decrease in case of reduction of cell viability. In principle, AuNPs may interfere with such a chromophore, generating additive absorption at 490 nm and hence, leading to an underestimation of the overall cytotoxicity. In the reality, the amount of Au internalized by the cells in each well (pg–ng range) is much lower than the amount of chromogenic substrate dispensed (hundreds of micrograms), thus it was easy to verify that the color generation was due to cell viability assessment rather than to the presence of AuNPs (Supplementary Information 6).

As shown in Figure 4, for both cell lines, Ctxb–AuNPs induced a small decrease in cell viability at a concentration of 100 µg Au ml^{-1}. This decrease was slightly more pronounced for A431 cells, which showed a 10% decrease when incubated with 25 µg Au ml^{-1} of Ctxb–AuNPs. At the same concentration, the viability of MDA-MB 453 cells was not affected. The toxicity increased with longer incubation times. For the scope of our work, we established that incubation with 5 µg Au ml^{-1} Ctxb–AuNPs during 30 min corresponds to a toxicity lower than 5%. These conditions were used for the experiments described in the manuscript. It must be noted that this concentration remained nontoxic for a longer incubation time (Supplementary Information 7).

Internalization & cell uptake of Ctxb–AuNPs

Chithrani *et al.* have shown that citrate-coated AuNPs might interact with serum proteins during incubation in cell culture medium and that nonspecific absorption of serum proteins onto bare AuNP may contribute to an appreciable AuNP cell uptake [37]. The cell uptake of the two different cell lines were analyzed by AAS for three different incubation conditions: cells incubated with Ctxb–AuNPs resuspended in cell culture medium (DMEM containing 10% FBS for 30 or 60 min); cells incubated with Ctxb–AuNPs resuspended in cell culture medium

10.2217/nnm-2018-0161

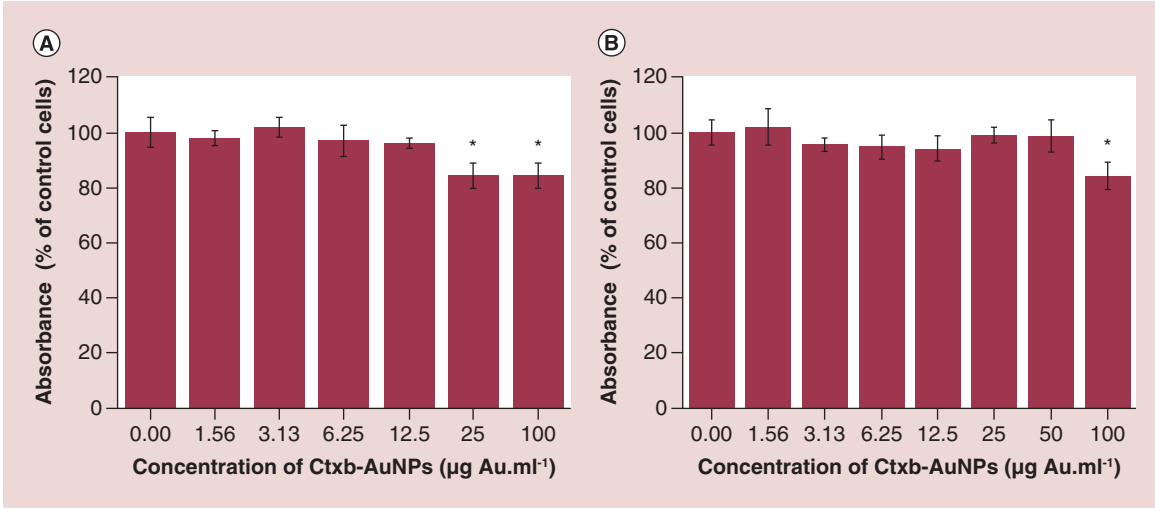

Figure 4. Cytotoxicity of AuNPs and Ctxb–AuNPs. A431 cells **(A)** or MDA-MB 453 cells **(B)** were incubated with different concentrations of Ctxb–AuNPs during 30 min and the number of viable cells was assessed by an MTS assay. Data are normalized to cells incubated in the same conditions without Ctxb–AuNPs and represent the mean absorbance ± 1 S.D. for n = 5 in one experiment. Results were statistically analyzed using a one-way ANOVA (Tukey test, *$p < 0.05$).
ANOVA: Analysis of variance; AuNP: Gold nanoparticle; Ctxb: Cetuximab; MTS: (3-(4,5-Dimethylthiazol-2-yl)-5-(3-carboxymethoxyphenyl)-2-(4-sulfophenyl)-2H-tetrazolium); S.D.: Standard deviation.

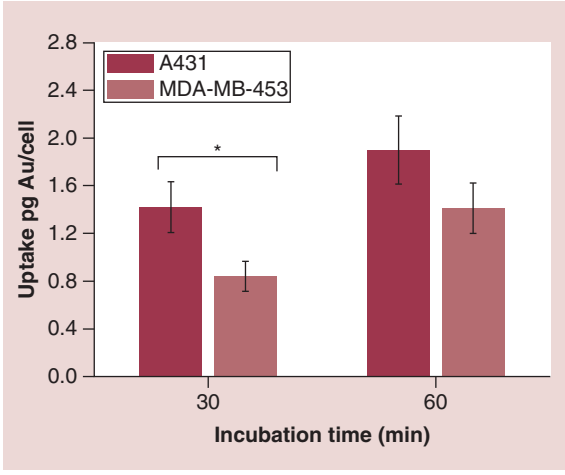

Figure 5. Determination of the gold content in cells exposed to gold nanoparticles conjugated with cetuximab. A431 and MDA-MB-453 cells were preincubated for 30 or 60 min with Ctxb–AuNPs at 5 µg Au ml^{-1}. After incubation, cells were washed, counted and digested by aqua regia. The amount of gold was quantified by AAS. Results are presented as mean ± 1 S.D. of three independent experiments. Results were analyzed using a one-way ANOVA (Tukey test, *$p < 0.05$).
AAS: Atomic absorption spectroscopy; ANOVA: Analysis of variance; AuNP: Gold nanoparticle; Ctxb: Cetuximab; S.D.: Standard deviation.

(DMEM containing 1% BSA for 15 or 30 min) and cells incubated with Ctxb–AuNPs resuspended in cell culture medium DMEM without any supplement (Supplementary Information 8).

Comparing these three conditions allows us to discriminate different NP–cell interactions. The analysis of AAS showed that there were three- to four-times higher cell internalization of the two cell lines for Ctxb–AuNPs resuspended in DMEM containing 10% FBS compared with DMEM alone. However, no marked difference regarding cell internalization between the two cell lines were observed for the media containing FBS or BSA. The GNP internalization in the presence of serum is mainly attributed to the presence of a protein corona surrounding the particles [38]. This serum protein-mediated internalization seems to be predominant compared with the specific receptor-mediated internalization. Thus, the cellular internalization of AuNPs was studied further by exposing Ctxb–AuNPs to A431 and MDA-MB-453 cells in the absence of serum proteins, followed by extensive washing to remove NPs adsorbed to the cell surface. AuNP uptake was quantified using AAS (Figure 5).

Receptor-mediated nanoparticle internalization is a rather rapid process compared with endocytic routes. Marega *et al.* have observed the cellular uptake of zeolite nanocrystals functionalized with Ctxb antibodies in the cells overexpressing the $EGFR^+$ already begins 15 min after incubation, at a rate around tenfold faster than that

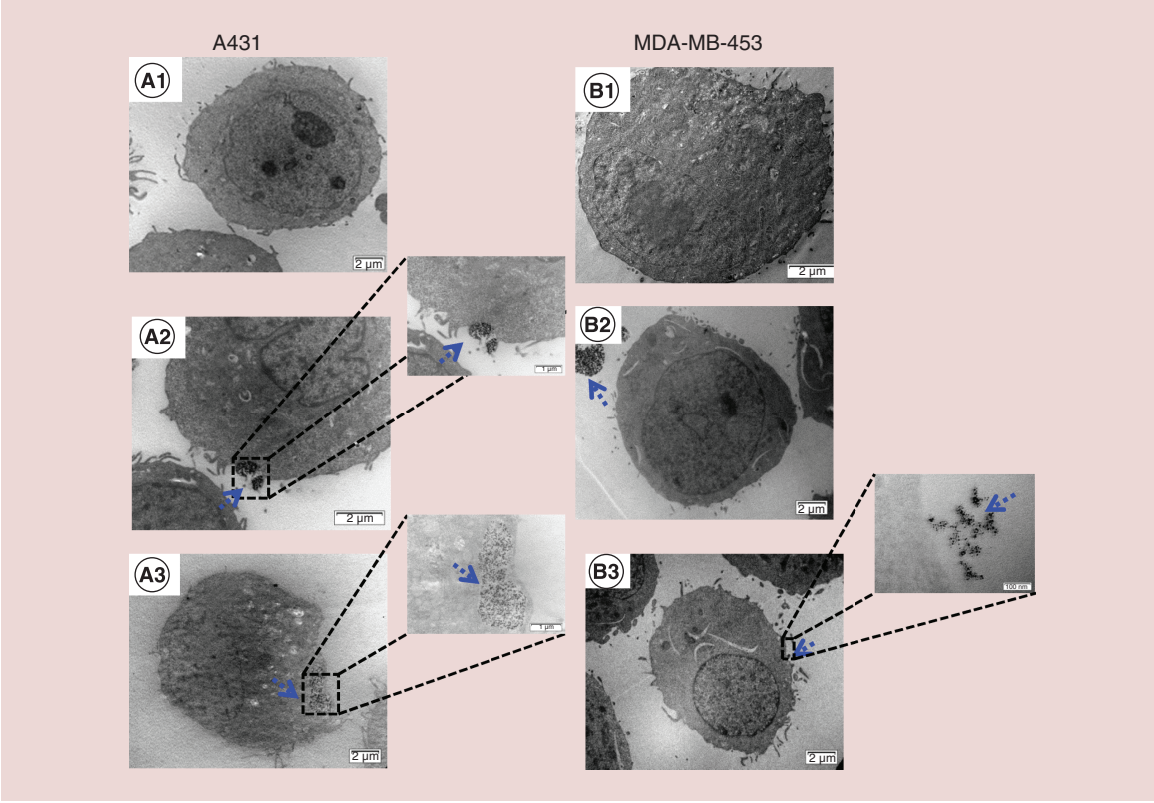

Figure 6. Transmission electron microscopy images of A431 and MDA-MB-453 cells. Control A431 cell **(A1)** or MDA-MB-435 cell **(B1)**, 5 µg Au ml^{-1} of Ctxb–AuNPs incubated 30 min with A431 cells **(A2 & A3)** or MDA-MB-435 cell **(B2 & B3)**. The scale bars are 2, 1 µm and 100 nm. Blue arrows indicate the localization of AuNPs. Images in the corners represent higher magnification images.
AuNP: Gold nanoparticle; Ctxb: Cetuximab.

observed in the negative control cells ($EGFR^-$) [36]. Thus, the significant internalization of Ctxb–AuNP at 30 min can be mainly attributed to fast receptor-mediated nanoparticle internalization that is not the case for MDA-MB 453 cells. However, when the incubation time is longer, in other words, for 1 h incubation, more than one processes (physical membrane permeation, endocytosis) can be involved in the nanoparticle internalization, which considerably contribute to the cell internalization in MDA-MB 453 cells. The fast receptor-mediated nanoparticle internalization process might explain the apparent difference of NPs internalization of A431 ($EGFR^+$) and MDA-MB 453 cells ($EGFR^-$) at a rather shorter (30 min) compared with longer incubation times (1 h).

Ctxb–AuNPs displayed a higher uptake in A431 cells compared with MDA-MB-453 cells at each time interval. After 30 min of incubation, 1.42 pg Au corresponding to about 1.1×10^6 AuNPs was internalized in each A431 cell, on average. This result suggests a rapid and efficient cell uptake of Ctxb–AuNPs mediated by ligand-receptor interaction. Unspecific binding of the AuNPs on the cell surface may explain the gold detected for MDA-MB-453 cells. The Ctxb–AuNPs uptake increased with incubation time for both cell lines. Furthermore, the uptake was much higher for Ctxb–AuNPs than for AuNPs (Supplementary Information 7). These data demonstrate that Ctxb–AuNPs were efficiently taken up by the EGFR-overexpressing cells A431, due to the proper binding ability of Ctxb to EGFR.

To confirm these data, the uptake of the Ctxb–AuNPs in A431 and MDA-MB-453 cells was also qualitatively observed by TEM (Figure 6). TEM images are not useful to assess the number of GNPs per cell. Indeed, 'ultrathin' sections from 50 to 100 nm thick are able to be viewed in the TEM and only a few cells are visible on a TEM grid. Furthermore, the objects that are observed are clusters of NPs and not individual NPs, hence, it is not possible to estimate the number of GNPs per cell by this technique. However, it gives useful information regarding their intracellular localization.

10.2217/nnm-2018-0161

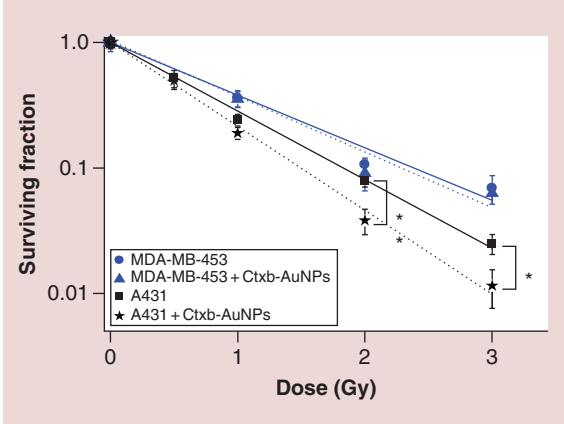

Figure 7. Survival curves of MDA-MB-453 cells and A431 cells incubated without gold nanoparticles conjugated with cetuximab (● solid line and ■ solid line, respectively) or preincubated 30 min with gold nanoparticles conjugated with cetuximab at 5 μg Au ml^{-1} (▲, dot line and ⋆ dot line, respectively). All the cells were then exposed to protons (LET = 25 keV μm^{-1}). Results are expressed as means ± 1 S.D. for 2–4 independent experiments, each performed in triplicates. Results were analyzed using a one-way ANOVA (Welch test, *$p < 0.05$, **$p < 0.01$).
ANOVA: Analysis of variance; LET: Linear energy transfer; S.D.: Standard deviation.

After incubation with 5 μg Au ml^{-1} of Ctxb–AuNPs for 30 min, black spots were observed both for A431cells or MDA-MB-453 cells, in cytoplasm and on the cell surface. However, A431 cells internalized a higher amount of Ctxb–AuNPs compared with MDA-MB-453 cells (Figure 6). Moreover, as shown in Figure 6 (a2), clusters of Ctxb–AuNPs were found around cellular extensions of A431 cell, which may indicate the recognition between the EGF receptors expressed in the plasma membrane of A431 cells and the Ctxb antibodies coupled to the AuNPs. The AuNPs seem to be bound on the cell surface and internalized probably by phagocytosis or receptor-mediated endocytosis since clusters of NPs are observed in membrane delineated vesicles (Supplementary Information 9). This recognition has not been observed neither for MDA-MB-453 cells, nor for A431 cells incubated with uncoupled AuNPs (Supplementary Information 9). The uptake, as measured by AAS, observed for MDA-MB-453 cells was thus probably due to unspecific binding of the AuNPs on the cell surface. For the TEM analysis, A431 cells and MDA-MB 453 cells were treated in parallel for comparison and incubated or not (control A1 and B1) with Ctxb–AuNPs for 30 min.

Altogether, these results suggest a specific internalization of Ctxb–AuNPs into A431 cells.

Radiosensitization effect of Ctxb–AuNPs

Irradiation experiment was performed to probe the possible radiosensitizing effects of Ctxb–AuNPs. For this purpose, A431 and MDA-MB-453 cells were incubated with a nontoxic concentration of 5 μg Au ml^{-1} Ctxb–AuNPs for 30 min and then irradiated by a proton beam. It should be noted that free Ctxb molecules (same concentration as in Ctxb–AuNPs) did not induce any change in cell survival upon irradiation at 2 Gy (data not shown). We chose to remove the NPs from the medium for the irradiation because we wanted to assess the effect of the NPs within the cells, without the interference of reactive oxygen species (ROS) that could be generated from the NPs in the culture medium. The radiosensitizing effect of Ctxb–AuNPs was quantified by standard *in vitro* clonogenic assays. The survival fractions were measured for doses ranging from 0 to 3 Gy upon irradiation with 25 keV μm^{-1} protons.

An exponential decrease in survival fraction for the cells irradiated by a proton beam of 25 keV μm^{-1} was observed (Figure 7). Survival fraction of MDA-MB-453 cells preincubated or not with Ctxb–AuNPs followed almost the same trend. However, the slope of the curve was higher for A431 cells preincubated with Ctxb–AuNPs compared with control A431 cells. A significant decrease in cell survival was already observed at 2 Gy, a clinically relevant radiation dose.

The efficiency of Ctxb–AuNPs to amplify radiation-induced A431 cell death was evaluated by calculating the SER at 10% survival. An SER value of 1.22 was obtained (Table 1). Our previous study demonstrated that 10-nm commercial amine-PEG-functionalized AuNPs amplified the cell death induced by 25 keV μm^{-1} proton beam radiation (SER was 1.14) [23]. In comparison, the cancer cell-targeting Ctxb–AuNPs developed in this study provided a higher SER than AuNPs.

Cell survival curves were fitted with a linear quadratic model. The coefficient α corresponds to the contribution of lesions, which are directly lethal for the cell, whereas β is attributed to the contribution of additive sublethal lesions. This last one was null for all conditions (Table 1).

Table 1. Calculated α coefficients and sensitization enhancement ratios for A431 and MDA-MB 453 cells irradiated with a proton beam at 25 keV μm^{-1} after being preincubated during 30 min with gold nanoparticles conjugated with cetuximab (5 μg Au ml^{-1}) as well as in control cells (without gold nanoparticles conjugated with cetuximab). The internalized gold nanoparticle quantities in each condition are reported in the last column.

Samples	α (Gy^{-1})	SER at 10% survival	AuNP quantities (Au pg/cell)
A431 (control)	1.26 (± 0.02)	–	0
A431 + Ctxb–AuNPs	1.54 (± 0.04)	1.22 (± 0.11)	1.42 (± 0.2)
MDA-MB-453 (control)	0.97 (± 0.06)	–	0
MDA-MB-453 + Ctxb–AuNPs	1.01 (± 0.07)	–	0.84 (± 0.1)

AuNP: Gold nanoparticle; Ctxb: Cetuximab; SER: Sensitization enhancement ratio.

This analysis showed that the presence of nanoparticles induced a 22% increase in the α parameter, indicating an enhancement of the lethality of the radiation treatment when Ctxb–AuNPs were added. This increase in cell killing is generally thought to be due to extra deposited dose from secondary electrons generated in the nanoparticles, subsequently giving rise to a local burst of ROS. *In silico* studies have demonstrated that this is indeed the case for spreadout Bragg peak (SBOP) protons, though to a lesser extent than when using kV photons. Using a modified Local Effect Model (LEM) approach, Lin *et al.* were able to predict SER for different nanoparticle distributions in a cell model and showed that AuNPs need to be close to a critical target, such as the cell nucleus, in order to get a significant effect when using a clinical proton beam [1]. Indeed, the range of secondary electrons produced in AuNPs is not sufficient to reach distant targets. This is even more relevant in this work, as the proton energy used (1.7 MeV) could only give rise to very low-energy electrons in AuNPs (hence nanometre-scale spike of ROS) and as the low number of these high-LET protons would limit the interaction probability with AuNPs. This issue questions the role of ROS in the radiosensitizing effect when using low-energy/high LET protons.

Hence, DMSO has been used to demonstrate the indirect effect of free radicals on cell killing with both photons and high LET particle radiation [4,23,39], a concentration of 1 M DMSO offering a maximal degree of protection, without having a toxic effect [40]. To address the role of ROS in the radiosensitizating effect of Ctxb–AuNPs in combination with protons, A431 cells were preincubated 30 min with or without 5 μg Au ml^{-1} of Ctxb–AuNPs. DMSO (1 M) was added just before the irradiation in some samples, kept during irradiation procedure and removed immediately after the 30-min incubation.

In the absence of Ctxb–AuNPs, cell survival increased from 2 to 18% when DMSO was added during the irradiation (Figure 8). It is a clear indication that the cell death induced by proton irradiation is partially caused by indirect action, in other words, production of free radicals by water radiolysis. In addition, we observed that, in the absence of scavenger, Ctxb–AuNPs contributed to 54% of cell death at 3 Gy. It decreased to 16% in the presence of radical scavenger. This corresponded to a decrease of 70% in the contribution of Ctxb-NPs to radiosensitization, when irradiation was performed in the presence of the radical scavenger. This finding further highlighted the possible role of Ctxb-NPs in enhancing the production of ROS in combination with low-energy protons, although this radiation quality was not initially expected to produce secondary electrons able to markedly ionize AuNPs.

Discussion

Our results demonstrate that the radiosensitization effect of AuNPs in combination with protons could be amplified with active targeting. The amount and specificity of gold accumulation in cancer cells can be greatly increased by conjugating AuNPs to Ctxb, a specific monoclonal antibody directed against EGFR. The higher uptake gives rise to a higher hit probability between the gold and incident proton tracks, resulting in the production of great amounts of extremely localized Auger and/or secondary electrons (within a range <100 nm) around nanoparticles. Due to the shorter-range secondary electrons produced for proton irradiation compared with x-rays, more action sites (internalized nanoparticles) are preferable in order to obtain a significant microscopic dose enhancement [41–43]. The dose enhancement, in principle, has two sources: direct ionization of critical cellular targets by the low-energy Auger electrons or secondary electrons (direct effects); ROS production generated by localized energy deposition (indirect effects).

While the exact mechanisms for AuNPs mediated radiosensitization with protons are yet to be fully elucidated, the ability of AuNPs to generate ROS along ion tracks and subsequent damage to critical cellular targets is worth to be investigated. An increased ROS production can be a direct consequence of a microscopic dose enhancement

10.2217/nnm-2018-0161

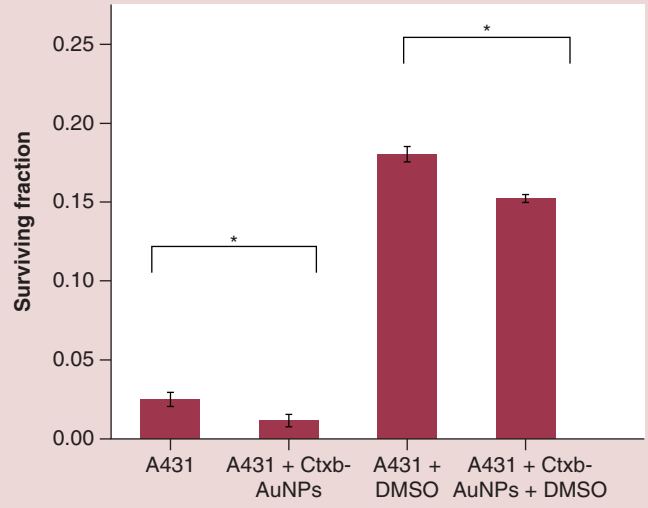

Figure 8. Survival fractions of A431 cells irradiated with 25 keV μm^{-1} proton beam at 3 Gy. A431 cells were preincubated or not for 30 min with Ctxb–AuNPs at 5 μg Au ml^{-1}. Cells were then irradiated in the presence or absence of DMSO that was added just before irradiation. Results are presented as mean ± S.D. for two independent experiments, each performed in triplicates. Results were statistically analyzed using a one-way ANOVA (Tukey test; *$p < 0.05$).
ANOVA: Analysis of variance; AuNP: Gold nanoparticle; Ctxb: Cetuximab; S.D.: Standard deviation.

(Auger electrons and secondary electrons) around Ctxb-NPs, as shown by Monte Carlo simulation studies [43,44]. As we showed that Ctxb–AuNPs are not essentially located in the close vicinity of nucleus, it can be hypothesized that the triggered ROS attack DNA by traveling through the nuclear membrane, or alter other crucial cell components in the cytoplasm.

So far, there have been limited reports on the radiosensitizating effects of nanoparticles in combination with ions. Porcel *et al.* have reported 11.3 and 18.5% enhancement of D50 (irradiation doses for 50% cell survival) values for Chinese hamster ovary cells treated with gadolinium-based nanoparticles and irradiated by C^{6+} or He^{2+}, respectively [45]. In another *in vitro* study, a dose reduction of 29% for C^{6+} irradiation is demonstrated for glucose-capped AuNPs-treated Hela cells as compared with untreated cells [46]. Kim *et al.* showed that internalized AuNPs decreased CT26 tumor cell survival in combination with 45 MeV proton beam [47]. As shown by those studies, a significant radiosensitization effect was observed for relatively higher concentration of nanoparticles (>0.1 mg ml^{-1}) and longer incubation time (few hours or overnight). Here, we showed a rapid and efficient cell uptake upon 30 min of incubation with 5 μg ml^{-1} of active targeting AuNPs. Moreover, the internalized Ctxb–AuNPs significantly enhanced the effect of proton radiation. In our previous report [23], the SER at 10% survival was 1.08 and 1.14 for A431 cells irradiated with protons of 25 keV μm^{-1} after being preincubated, respectively, with bare untargeted 5 or 10 nm AuNPs at 50 μg Au ml^{-1} for 24 h. In the present study, the SER at 10% survival was 1.22 for targeted Ctxb–AuNPs at 5 μg Au ml^{-1} for 30 min, demonstrating the much higher effect due to active targeting. The active targeting of such Ctxb-coupled nanoparticles toward EGFR-expressing A431 cells has already been demonstrated *in vitro* and *in vivo* [30].

Low-energy protons used in this work (25 keV μm^{-1}) are of interest clinically because a proportion of beam energy in the spread out Bragg peak will be below 10 MeV. The radiosensitization provided by AuNPs in the distal part of the tumor would be highly dependent on those low-energy protons. This is particularly important as different beam qualities do not provide the same effect (as shown in our previous work [23]). A variation of SER could potentially be observed along tumor depth *in vivo*. It is the first proof of concept that actively targeting nanoparticles may be used for proton therapy.

Conclusion & future perspective

Significant progress has been made in the development of new agents and new strategies against cancer. Yet, the major challenge remains in targeting and selectively killing cancer cells while affecting as few healthy cells as possible.

In this work, we demonstrate that AuNPs conjugated to tumor-targeting moieties can bind to cancer cells with high affinity and specificity. Moreover, they amplify cell death with proton ions used as ionizing radiations. It evidences the feasibility of adopting a novel protocol of combining protontherapy with tumor-targeting nanomedicine in cancer treatment. This finding impacts the strategy to develop targeted cancer nanotherapy and treatment planning aimed at improving proton ion treatments, ultimately, reducing negative radiation effects in healthy tissues in front of the tumor. This strategy is at its start and requires many more improvements. The efficacy and biodistribution of nanoparticles must be further optimized to be of clinical interest for radio-oncologists. Finally, the ideal combination (proton dose and sequence of treatment) still needs to be defined.

Summary points

- Approximately two to three cetuximab (Ctxb) molecules were conjugated to each gold nanoparticle (AuNP).
- Ctxb–AuNPs specifically bind to EGFR-overexpressing A431 cells, but not to EGFR-negative MDA-MB-453 cells.
- Transmission electron microscopy analysis evidenced the accumulation of Ctxb–AuNPs in the cell membrane region and cytoplasm of A431 cells.
- Uptake, quantified by atomic adsorption spectroscopy, showed higher gold quantity in A431 cells compared with MDA-MB-453 cells.
- Ctxb–AuNPs significantly enhanced the effect of proton irradiation in A431 cells but not in MDA-MB-453 cells.
- The radiosensitizing effect of Ctxb–AuNPs was higher than with unconjugated AuNPs.

Supplementary data

To view the supplementary data that accompany this paper please visit the journal website at: www.futuremedicine.com/doi/full/10.2217/nnm-2018-0161

Acknowledgments

The authors thank the 'Morphology-Imaging' technological platform of the University of Namur for the electron microscopy. The authors also acknowledge the support of the SIAM platform. Sébastien Penninckx is a PhD fellow funded by the Belgian Funds for Scientific Research (FRS-FNRS, Belgium).

Ethical conduct of research

The authors state that they have obtained appropriate institutional review board approval or have followed the principles outlined in the Declaration of Helsinki for all human or animal experimental investigations. In addition, for investigations involving human subjects, informed consent has been obtained from the participants involved.

Financial & competing interests disclosure

TheraPlus project was supported by the Walloon Region (grant 1318075). The authors have no other relevant affiliations or financial involvement with any organization or entity with a financial interest in or financial conflict with the subject matter or materials discussed in the manuscript apart from those disclosed.

No writing assistance was utilized in the production of this manuscript.

References

Papers of special note have been highlighted as: • of interest; •• of considerable interest

1. Lin Y, McMahon SJ, Scarpelli M, Paganetti H, Schuemann J. Comparing gold nano-particle enhanced radiotherapy with protons, megavoltage photons and kilovoltage photons: a Monte Carlo simulation. *Phys. Med. Biol.* 59(24), 7675–7689 (2014).
2. Lin Y, Paganetti H, McMahon SJ, Schuemann J. Gold nanoparticle induced vasculature damage in radiotherapy: comparing protons, megavoltage photons, and kilovoltage photons. *Med. Phys.* 42(10), 5890–5902 (2015).
3. Hainfeld JF, Dilmanian FA, Slatkin DN, Smilowitz HM. Radiotherapy enhancement with gold nanoparticles. *J. Pharm. Pharmacol.* 60(8), 977–985 (2008).
4. Jeynes JC, Merchant MJ, Spindler A, Wera AC, Kirkby KJ. Investigation of gold nanoparticle radiosensitization mechanisms using a free radical scavenger and protons of different energies. *Phys. Med. Biol.* 59(21), 6431–6443 (2014).
5. Polf JC, Bronk LF, Driessen WH *et al.* Enhanced relative biological effectiveness of proton radiotherapy in tumor cells with internalized gold nanoparticles. *Appl. Phys. Lett.* 98(19), 193702 (2011).

6. Shrestha S, Cooper LN, Andreev OA, Reshetnyal YK, Antosh MP. Gold nanoparticles for radiation enhancement *in vivo*. *Jacobs J. Radiat. Oncol.* 7(8), 026 (2016).
7. Haume K, Rosa S, Grellet S *et al.* Gold nanoparticles for cancer radiotherapy: a review. *Cancer Nanotechnol.* 7(1), 8 (2016).

•• **Extensive review of the potential of gold nanoparticles (AuNPs) for cancer therapy.**

8. Porcel E, Liehn S, Remita H *et al.* Platinum nanoparticles: a promising material for future cancer therapy? *Nanotechnology* 21(8), 85103 (2010).
9. McMahon SJ, Hyland WB, Muir MF *et al.* Biological consequences of nanoscale energy deposition near irradiated heavy atom nanoparticles. *Sci. Rep.* 1, 18 (2011).
10. Hainfeld JF, Slatkin DN, Smilowitz HM. The use of gold nanoparticles to enhance radiotherapy in mice. *Phys. Med. Biol.* 49(18), N309–15 (2004).

• **One of the first reports to evidence nanoparticle-mediated radiosensitization *in vivo*.**

11. Zhong Y, Meng F, Deng C, Zhong Z. Ligand-directed active tumor-targeting polymeric nanoparticles for cancer chemotherapy. *Biomacromolecules* 15(6), 1955–1969 (2014).
12. Arteaga C. Targeting HER1/EGFR: a molecular approach to cancer therapy. *Semin. Oncol.* 30(3 Suppl. 7), 3–14 (2003).
13. Grandis JR, Sok JC. Signaling through the epidermal growth factor receptor during the development of malignancy. *Pharmacol. Ther.* 102(1), 37–46 (2004).
14. Liu J, Liang Y, Liu T, Li D, Yang X. Anti-EGFR-conjugated hollow gold nanospheres enhance radiocytotoxic targeting of cervical cancer at megavoltage radiation energies. *Nanoscale Res. Lett.* 10, 218 (2015).
15. Zimmermann M, Zouhair A, Azria D, Ozsahin M. The epidermal growth factor receptor (EGFR) in head and neck cancer: its role and treatment implications. *Radiat. Oncol.* 1, 11 (2006).
16. Yewale C, Baradia D, Vhora I, Patil S, Misra A. Epidermal growth factor receptor targeting in cancer: a review of trends and strategies. *Biomaterials* 34(34), 8690–8707 (2013).
17. Galizia G, Lieto E, De Vita F *et al.* Cetuximab, a chimeric human mouse anti-epidermal growth factor receptor monoclonal antibody, in the treatment of human colorectal cancer. *Oncogene* 26(25), 3654–3660 (2007).
18. Martinelli E, De Palma R, Orditura M, De Vita F, Ciardiello F. Anti-epidermal growth factor receptor monoclonal antibodies in cancer therapy. *Clin. Exp. Immunol.* 158(1), 1–9 (2009).
19. Qian Y, Qiu M, Wu Q *et al.* Enhanced cytotoxic activity of cetuximab in EGFR-positive lung cancer by conjugating with gold nanoparticles. *Sci. Rep.* 4, 7490 (2014).
20. Kao HW, Lin YY, Chen CC *et al.* Biological characterization of cetuximab-conjugated gold nanoparticles in a tumor animal model. *Nanotechnology* 25(29), 295102 (2014).
21. Karmani L, Labar D, Valembois V *et al.* Antibody-functionalized nanoparticles for imaging cancer: influence of conjugation to gold nanoparticles on the biodistribution of 89Zr-labeled cetuximab in mice. *Contrast Media Mol. Imaging* 8(5), 402–408 (2013).

• **Biodistribution and tumor accumulation of AuNPs conjugated with cetuximab.**

22. Kao HW, Lin YY, Chen CC *et al.* Evaluation of EGFR-targeted radioimmuno-gold-nanoparticles as a theranostic agent in a tumor animal model. *Bioorg. Med. Chem. Lett.* 23(11), 3180–3185 (2013).
23. Li S, Penninckx S, Karmani L *et al.* LET-dependent radiosensitization effects of gold nanoparticles for proton irradiation. *Nanotechnology* 27(45), 455101 (2016).
24. Walzlein C, Scifoni E, Kramer M, Durante M. Simulations of dose enhancement for heavy atom nanoparticles irradiated by protons. *Phys. Med. Biol.* 59(6), 1441–1458 (2014).
25. Moreau N, Michiels C, Masereel B *et al.* PVD synthesis and transfer into water-based solutions of functionalized gold nanoparticles. *Plasma Proc. Polym.* 6(S1), 5888–5892 (2009).
26. Dynamic light scattering – common terms defined Malvern Instruments Worldwide http://docplayer.net/15065673-Dynamic-light-scattering-common-terms-defined.html
27. Janmaat ML, Kruyt FA, Rodriguez JA, Giaccone G. Response to epidermal growth factor receptor inhibitors in non-small cell lung cancer cells: limited antiproliferative effects and absence of apoptosis associated with persistent activity of extracellular signal-regulated kinase or Akt kinase pathways. *Clin. Cancer Res.* 9(6), 2316–2326 (2003).
28. Meira DD, Nobrega I, de Almeida VH *et al.* Different antiproliferative effects of matuzumab and cetuximab in A431 cells are associated with persistent activity of the MAPK pathway. *Eur. J. Cancer* 45(7), 1265–1273 (2009).
29. Subik K, Lee JF, Baxter L *et al.* The expression patterns of ER, PR, HER2, CK5/6, EGFR, Ki-67 and AR by immunohistochemical analysis in breast cancer cell lines. *Breast Cancer (Auckl.)* 435–441 (2010).
30. Marega R, Karmani L, Flamant L *et al.* Antibody-functionalized polymer-coated gold nanoparticles targeting cancer cells: an *in vitro* and *in vivo* study. *J. Mat. Chem.* 22(39), 21305–12312 (2012).
31. Piret JP, Jacques D, Audinot JN *et al.* Copper(II) oxide nanoparticles penetrate into HepG2 cells, exert cytotoxicity via oxidative stress and induce pro-inflammatory response. *Nanoscale* 4(22), 7168–7184 (2012).

32. Wera AC, Riquier H, Heuskin AC, Michiels C, Lucas S. *In vitro* irradiation station for broad beam radiobiological experiments. *Nucl. Instruments Phys. Res. B.* 269(24), 3120–3124 (2011).
33. Ziegler JF. *The Stopping and Range of Ions in Matter*. Springer, MA, USA (1985).
34. Turner J. *Atoms, Radiation, and Radiation Protection*. Wiley-VCH Verlag GmbH & Co., KGaA, Germany (1995).
35. Pineux F, Marega R, Stopin A *et al.* Biotechnological promises of Fe-filled CNTs for cell shepherding and magnetic fluid hyperthermia applications. *Nanoscale* 7(48), 20474–20488 (2015).
36. Marega R, Prasetyanto EA, Michiels C, De Cola L, Bonifazi D. Fast targeting and cancer cell uptake of luminescent antibody-nanozeolite bioconjugates. *Small* 12(39), 5431–5441 (2016).
37. Chithrani BD, Ghazani AA, Chan WC. Determining the size and shape dependence of gold nanoparticle uptake into mammalian cells. *Nano Lett.* 6(4), 662–668 (2006).
38. Safi M, Courtois J, Seigneuret M, Conjeaud H, Berret JF. The effects of aggregation and protein corona on the cellular internalization of iron oxide nanoparticles. *Biomaterials* 32(35), 9353–9363 (2011).
39. Porcel E, Li S, Usami N *et al.* Nano-sensitization under gamma rays and fast ion radiation. *J. Phys.: Conf. Series* 373(1), 012006 (2012).
40. Hirayama R, Matsumoto Y, Uzawa A *et al.* Indirect action to cell killing by SOBP carbon-ion beams. *J. Rad. Res.* 55(Suppl. 1), i133–i134 (2014).
41. Lin Y, McMahon SJ, Paganetti H, Schuemann J. Biological modeling of gold nanoparticle enhanced radiotherapy for proton therapy. *Phys. Med. Biol.* 60(10), 4149–4168 (2015).

- **Monte Carlo simulations suggest that vasculature damage can be induced and may participate to tumor eradication.**

42. Ahmad R, Royle G, Lourenço A *et al.* Investigation into the effects of high-Z nano materials in proton therapy. *Phys. Med. Biol.* 61(12), 4537–4550 (2016).
43. Cho J, Gonzalez-Lepera C, Manohar N *et al.* Quantitative investigation of physical factors contributing to gold nanoparticle-mediated proton dose enhancement. *Phys. Med. Biol.* 61(6), 2562–2581 (2016).
44. Heuskin AC, Gallez B, Feron O *et al.* Metallic nanoparticles irradiated by low-energy protons for radiation therapy: are there significant physical effects to enhance the dose delivery? *Med. Phys.* 44(8), 4299–4312 (2017).
45. Porcel E, Tillement O, Lux F *et al.* Gadolinium-based nanoparticles to improve the hadrontherapy performances. *Nanomedicine* 10(8), 1601–1608 (2014).
46. Kaur H, Pujari G, Semwal MK, Sarma A, Avasthi DK. *In vitro* studies on radiosensitization effect of glucose capped gold nanoparticles in photon and ion irradiation of HeLa cells. *Nucl. Instruments Phys. Res. B* 3017–3011 (2013).
47. Kim JK, Seo SJ, Kim KH *et al.* Therapeutic application of metallic nanoparticles combined with particle-induced x-ray emission effect. *Nanotechnology* 21(42), 425102 (2010).